Eur. Phys. J. B **22**, 307–320 (2001)

**THE EUROPEAN PHYSICAL JOURNAL B**

EDP Sciences


# Determination of SWCNT diameters from the Raman response of the radial breathing mode

H. Kuzmany[1,a], W. Plank[1], M. Hulman[1], Ch. Kramberger[1], A. Grüneis[1], Th. Pichler[1,2], H. Peterlik[1], H. Kataura[3], and Y. Achiba[4]

[1] Universität Wien, Institut für Materialphysik, Strudlhofgasse 4, 1090 Wien, Austria
[2] Institut für Festkoerperphysik und Werkstofforschung, Dresden, Germany
[3] Department of Physics, Tokyo Metropolitan University, Tokyo, Japan
[4] Department of Chemistry, Tokyo Metropolitan University, Tokyo, Japan

Received 18 February 2001 and Received in final form 3 April 2001

**Abstract.** We report on the evaluation of the distribution of diameters for nanotube samples with a wide variation of mean diameters. Such results were obtained from a detailed analysis of the radial breathing mode Raman response and compared to results obtained from an evaluation of optical spectra and X-ray diffraction pattern. The evaluation of the Raman data needs a well refined analysis as the experimental analysis exhibits a rather complicated and oscillating relation between response and exciting laser. Both, an exact calculation where the density of states was considered explicitly and an approximate calculation were applied. Both models used for the analysis are able to explain several unexpected results from the experiment such as the oscillating behavior of the spectral moments, unusual discontinuities in the first moments of the Raman response for excitation in the IR, a fine structure for the response in optics and Raman, and an up shift of the RBM frequency as compared to qualified *ab initio* calculations. In detail the first moment and the variance of the spectra were used for the evaluation of the diameter distribution. To obtain good results between experimental and theoretical oscillation pattern the transition energy between the first two van Hove singularities had to be scaled up which is considered as a result from coulomb interaction of the electrons in the tubular material. On the other hand the analysis does not only allow to determine the mean value and the width of the diameter distribution but yields also a value for the average bundle diameters or, alternatively, the strength of the tube-tube interaction. The model used for the analysis of the Raman data is also appropriate to analyze the optical response, at least for the spectral range from 0.5 eV to 3.5 eV. The fine structure in the response for the transitions between the three lowest van Hove singularities is well reproduced and the mean tube diameters and their distribution is obtained in very good agreement with the results from the Raman analysis. From the X-ray analysis the same mean values and comparable distributions for the tube diameters were received whereas the bundle diameters could not be retained with high precision in this case.

**PACS.** 61.46.+w Nanoscale materials: clusters, nanoparticles, nanotubes, and nanocrystals – 63.20.Dj Phonon states and bands, normal modes, and phonon dispersion – 78.30.-j Infrared and Raman spectra

## 1 Introduction

Carbon nanotubes as discovered in 1991 by Iijima *et al.* [1] exhibit a multiwall structure consisting of several concentric rolled up graphene planes. Structure and properties of such tubes are difficult to analyze since contributions of the various shells mix and can hardly be separated. Only after a successful preparation of large quantities of single-wall carbon nanotubes (SWCNTs) by Thess *et al.* [2] and later on by Journet *et al.* [3] and other groups, research expanded dramatically [4]. The single, rolled up graphene plane can be considered as an one dimensional (1D) electronic systems. Each tube is described by a lattice vector $(n, m)$ in the graphene plane which turns into the circumference of the tube on rolling up the sheet. $n, m$ are integers and are called the components of the *Hamada vector* or *folding vector*. Dividing the length of the Hamada vector by $\pi$ yields the diameter of the tube. Likewise, $n$ and $m$ determine the helicity of the rolled up sheet. Within a certain diameter range a rather large number of tubes with different helicities is geometrically allowed which yields an almost continuous distribution of possible diameters. There is good evidence and wide agreement that for certain preparation conditions all geometrically allowed tubes

[a] e-mail: kuzman@ap.univie.ac.at

are grown and any selection comes only from the tube diameter [5–8]. This is agreed even though Raman spectra and optical absorption exhibit a fine structure which can be fitted with a rather small number of individual oscillators. These oscillators were ascribed in some early work to a selective collection of certain tube diameters [9–11] and could thus indicate selective tube growth. By varying growth temperature and catalyst tube material with a mean diameter between 0.9 nm 1.5 nm could be grown so far [12,13]. In extreme cases where the tubes were grown in the cavities of a zeolite tube diameters as small as 0.4 nm have been reported [14].

The electronic properties of the nanotubes are obtained from a zone folding procedure in the graphene plane. Electrons can accommodate quasicontinuous $k$-vectors along the tube axis but are trapped into well separated $k$-vectors perpendicular to this axis. The ideal, defect-less SWCNT thus exhibits typical 1D van Hove singularities in the density of electronic states (DOS). For optical absorption only symmetric transitions between singularities from the valence band to singularities in the conduction band are allowed. The number of singularities in the DOS scales up with the diameter of the tubes but it is independent from their helicity. Electronic transition energies scale with the $\pi$-$\pi$ overlap integral $\gamma_0$. The value for the latter is 2.5 eV as calculated for the graphene plane in a tight binding approximation where only $\pi$-orbitals are considered. For the nanotubes best agreement with experiments has been obtained for a value between 2.9 and 3 eV [8,9,15]. For such values the first two allowed optical transitions for tubes with a standard diameter of 1.36 nm will occur at 0.7 and 1.2 eV in semiconducting tubes and at 1.9 eV for the first allowed transition in metallic tubes. The positions of the van Hove singularities and thus the transition energies scale up linearly with the inverse of the tube diameter [12,16,17].

Experimental values for the tube diameters were first obtained from X-ray analysis of nanotube bundles [2]. Subtracting a van der Waals distance of 0.3 nm from the evaluated center to center separation of the tubes a tube diameter in reasonable good agreement with statistical values from a TEM analysis was obtained [2]. Also, the average position of the absorption bands from thin films have been used successfully to obtain a good estimate for the average tube diameter [12].

The Raman spectrum of SWCNTs has two important regions. The first one around 1580 $\mathrm{cm}^{-1}$ is strongly related to the tangential Raman mode in graphite. The second one between 140 and 220 $\mathrm{cm}^{-1}$ originates from a radial breathing mode (RBM) and is unique for SWCNTs. Its position and shape depends strongly on the exciting laser wavelength as demonstrated for the first time by Rao *et al.* [18]. This was explained by a photo-selective resonance scattering of the modes. Each laser selects resonantly those tubes for which the electronic transitions match best with the laser energy. Like the transition energies, the RBM frequencies also scale inverse with the tube diameter. Since the original work of Rao *et al.* the unusual response of this line in the Raman spectra has been discussed in several hundred papers. *Ab initio* calculations confirmed the $1/d$ dependence of the mode frequency [19,20] and yielded an appropriate factor of proportionality. This has motivated several authors to use Raman results from the RBM for the analysis of tube diameters as well. A problem for such analyzes arises certainly from the large differences in the average and peak line positions if different lasers are used for excitation. Only very recently a better understanding for the response of the RBM was obtained from an extended experimental and theoretical analysis of the response [8,17]. The response of the peak position and of the first and second moments of the spectra were found in reference [17] to oscillate with the energy of the exciting laser. This oscillation was found to be due to the macroscopic quantization of the electronic levels as a consequence of the finite size of the tubes in direction perpendicular to the tube axis and due to the distribution of the states along the tube axis into van Hove singularities. Furthermore, in the latter work a useful approximation was developed which allowed to evaluate the spectral moments for the Raman response of the RBM without explicit use of the joined density of states. This simplified model was used to determine the mean and the width of the diameter distribution of a SWCNT sample. The knowledge of the first and second moment of the spectral distribution for excitation with only one laser line was demonstrated to be sufficient for this.

On account of the above described results it was certainly demanding to check the range of validity for the two developed models and to apply them to samples with different mean diameters. In this paper we present therefore a detailed version of the mathematical background for the two models and the pitfalls which must be known for the evaluation of diameters from the RBM. The exact model which uses explicitly the DOS for all geometrically allowed tubes is related to the approximate evaluation where only the resonance positions are considered as a continuous distribution. For the evaluation of the first and second spectral moments the different models yield almost the same result for standard tubes. Discrepancies are found for very thin tubes with diameters below 1 nm. The consequences of the oscillating behavior of the moments with respect to the energy of the exciting laser are discussed and the unusual response observed for several laser lines is explained. The model for the analysis is applied to nanotubes with 6 different mean diameters. Good agreement with the experiment is only obtained if the energies for the two lowest transitions are scaled up by about 10% from their tight binding value. Both, the model which uses the full DOS and the approximate model are also applied to interpret spectra for optical absorption and to derive the mean diameters and their distribution. Almost the same type of up scale is requested in this case as for the Raman spectra. The fine structure observed in the optical spectra is well reproduced by the model. Results for the diameters are found in very good agreement with the results from the evaluation of the Raman data and from a detailed X-ray analysis but thin tube material needs a special treatment. Average diameters of carbon nanotube

$$\epsilon_{n,m}(k) = \pm\,\gamma_0 \left\{ 1 + 2\left[ (-1)^{\frac{2n+m}{d_R}} \cos\left( \frac{\sqrt{3}ka}{2} \frac{m}{(n^2+m^2+nm)^{1/2}} + q\pi \frac{2n+m}{n^2+m^2+nm} \right) \right.\right.$$
$$+ (-1)^{\frac{n+2m}{d_R}} \cos\left( -\frac{\sqrt{3}ka}{2} \frac{n}{(n^2+m^2+nm)^{1/2}} + q\pi \frac{n+2m}{n^2+m^2+nm} \right)\Big]$$
$$\left. + 2\left[ 1 + (-1)^{\frac{n-m}{d_R}} \cos\left( \frac{\sqrt{3}ka}{2} \frac{n+m}{(n^2+m^2+nm)^{1/2}} + q\pi \frac{n-m}{n^2+m^2+nm} \right) \right] \right\}^{1/2}, \quad (2)$$

bundles could only be determined from the Raman data but their quantitative value relies on details of the theory used for the evaluation. The fine structure in both, the Raman response and the optical response is found to be due to a clustering of diameters as a consequence of their small value.

## 2 Evaluation of Raman intensities and spectral moments, basic relations

The evaluation of the Raman spectra was performed in several steps. First the frequency of the RBM was calculated using an *ab initio* program package. Then the density of states was evaluated for all geometrically allowed modes between 0.5 nm and 2.0 nm diameter within a tight binding approximation. With these results a theory for resonance Raman scattering was applied to evaluate spectral intensities and their moments. Finally, a continuum approximation is used to evaluate the spectral moments and to determine the parameters of the distribution function.

### 2.1 Evaluation of mode frequencies and density of states

For the evaluation of the mode frequencies $\nu_{\mathrm{RBM}}$ the results obtained from the *Vienna ab initio simulation package* were used as reported previously [20]. The package allows only to calculate armchair tubes ($n = m$) and zigzag tubes ($n$ or $m = 0$) in the requested diameter range. From an interpolation of the form $\nu_{\mathrm{RBM}} = [239 - 5(n-m)]/d(n,m)$ one can obtain safely the RBM frequencies for arbitrary helicities. Within the limits of the accuracy of the calculation and to be consistent with the various analyzes performed in the present work we have used a constant value of 234 $\mathrm{cm}^{-1}$nm for the factor of proportionality between the RBM frequency of a single tube and $1/d$.

The RBM frequency is known to be up shifted by intertube interaction in the bundles. Several recent calculations estimate this up shift to be between 8% and 12% for typically (10,10) tube diameters [21,23]. From additional theoretical analyzes this up shift was found to depend on the diameter of the tubes $d$ and on the number $N$ of tubes in the bundles [22]. Hence, to obtain best agreement with details of the analysis we have used

$$\nu_{\mathrm{RBM}}(n,m) = \frac{234}{d(n,m)} + C_2(N,d) \quad (1)$$

for the RBM frequency in this work. $C_2$ is a function to describe the tube-tube interaction as discussed in detail in Section 6.3.

The density of states was evaluated for all geometrically allowed tubes from zone folding the tight binding band structure

*See equation (2) above*

where $\gamma_0 \approx 2.9$ eV and $a = 2.46$ Å are the carbon-carbon interaction energy and the lattice constant of the graphene sheet, respectively. $d_R$ is the greatest common divisor of $(2n + m)$ and $(n + 2m)$ and $q$ is the subband index extending from $\{-(n^2 + m^2 + nm)/d_R\}$ to $\{(n^2 + m^2 + nm)/d_R - 1\}$. For each subband $k$ extends from $-\pi/T$ to $\pi/T$, where $T$ is the length of the unit cell.

The density of sates was evaluated for every 10 meV. To avoid instabilities in the calculations the resulting divergencies were cut off at a factor of 100 above their average value and subsequently smoothed by a 6 point gliding average. This procedure considers the finite effective width of the electronic states due to life time effects and spectral resolution.

### 2.2 Calculation of Raman intensities and spectral moments by using the density of states explicitly

For the evaluation of the resonance Raman intensities the theory of Martin and Falicov [24] is used. The Feynman diagram yields for the normalized matrix elements of a one phonon Raman process

$$K_{2f,10} = \sum_{ji} \frac{M_{fj} M_{ji} M_{i0}}{(\hbar\omega_1 - \epsilon_j - \mathrm{i}\hbar\alpha)(\hbar\omega_2 - \epsilon_l - \mathrm{i}\hbar\alpha)}, \quad (3)$$

where 0 and $f$ assign the initial state with a photon $\omega_1 = \omega_i$ and the final state with a photon $\omega_2 = \omega_s$ and a phonon $\pm\nu = \omega_2 - \omega_1$, respectively. The first and the third matrix element in the equation describe the electron-photon coupling. The matrix element in the center originates from the electron-phonon interaction where one phonon is created, and $1/\alpha$ is the lifetime of the excited state. $i$ and $j$ assign intermediate states with and without a phonon. The denominator expresses the resonances for the incoming and for the outgoing photon. The scattering cross section $\sigma(\omega_i)$ is proportional to the absolute square of the expression in equation (3). In a solid there is a continuous possibility for transitions from the valence band to the conduction band which means the sum in

equation (3) can be replaced by an integral over the joint density of states $g_{\rm jds}(\epsilon)$ and the scattering cross section becomes

$$\sigma(\omega_i) \propto \left| \int \frac{M_{\rm f} M_{\rm ph} M_0 g_{\rm jds}(n,m,\epsilon) {\rm d}\epsilon}{(\hbar\omega_i - \epsilon - {\rm i}\hbar\alpha)(\hbar\omega_s - \epsilon - {\rm i}\hbar\alpha)} \right|^2 \quad (4)$$

where the three symbols $M_{\rm f}, M_{\rm ph}$, and $M_0$ represent the three matrix elements from equation (3). For matrix elements which depend weakly on the energy as compared to the denominators in equation (3) or equation (4) the triple product of the matrix elements can be removed from the integral. In this case the spectral intensity for a set of tubes $(n,m)$ with Gaussian distributed diameters $d_{n,m}$ is obtained from

$$I_0(\nu) = \sum_{n,m} \left\{ L(\nu, \nu(n,m), \Gamma) \exp\left[ -\frac{(d_{n,m} - d_0)^2}{2\sigma^2} \right] \times \left| \int \frac{g_{\rm jds}(n,m,\epsilon)\, {\rm d}\epsilon}{(\hbar\omega_{\rm i} - \epsilon - {\rm i}\hbar\alpha)(\hbar\omega_{\rm s} - \epsilon - {\rm i}\hbar\alpha)} \right|^2 \right\}. \quad (5)$$

$L(\nu, \nu(n,m), \Gamma)$ is a line shape function for the phonon mode of tube $(n,m)$ with width $\Gamma$. For the discussion performed below $\hbar\alpha = 0.01$ eV was assumed and a Lorentzian line was used for $L$. $d_0$ and $\sigma^2$ are the mean and the variance of the Gaussian function describing the diameter distribution of the sample [8,10,17]. The variance is related to the FWHM as $\sigma^2 = FWHM^2/8\ln 2$. $g_{\rm jds}(n,m,\epsilon)$ is the DOS from Section 2.1 with $\epsilon$ replaced by $2\epsilon$. Equation (5) allows immediately to calculate the first moment from

$$\langle \nu(\epsilon) \rangle = \frac{\int \nu I_0(\nu) {\rm d}\nu}{\int I_0(\nu) {\rm d}\nu} \quad (6)$$

and the spectral variance from

$$\Delta(\nu) = \langle \nu^2 \rangle - \langle \nu \rangle^2, \quad (7)$$

both as function of the excitation energy $\hbar\omega_i$. The evaluation of the spectral moments according to the above model will be assigned in the following as *full DOS* calculation.

### 2.3 Continuum approximation of spectral moments

Since the van Hove singularities dominate the spectral response one can substitute the explicit DOS function by a constant value for each tube and thus drop the integration over the energy in equation (5). Considering only the first 8 transitions we obtain for the first moment

$$\langle \nu(\epsilon) \rangle = \frac{\sum_{j=1}^{8} \int_{a_{j-}}^{a_{j+}} [\nu_{\rm RBM} + C_2(N,d)]\, \rho(d) \exp[-(d-d_0)^2/2\sigma^2]\, {\rm d}d}{\sum_{j=1}^{8} \int_{a_{j-}}^{a_{j+}} \rho(d) \exp[-(d-d_0)^2/2\sigma^2]\, {\rm d}d}. \quad (8)$$

The integration extends over a range determined by the upper and lower border lines for each van Hove singularity which limit the relation between $1/d$ and $\epsilon$. For the $j$th singularity these borderlines can be evaluated from the theory of [16] and have the form

$$a_{j\pm}(\epsilon) = (2j g_j a_{\rm CC} \gamma_0 / d) \pm j a_{\rm CC}/6,$$

where $a_{CC} = 1.44$ Å is the C-C separation in the graphene sheet.

$$\rho(d) = \Delta Z(d)/\Delta d = \frac{d(n,m)\pi^3}{9\sqrt{3} a_{\rm CC}^2} \quad (9)$$

is the continuum description for the density of tube diameters as derived from the total number $Z(d(n,m))$ of tubes in a diameter range from 0 to $d$. $g_j = 1.1$ for $j = 1, 2$ and 1 otherwise. It is considered as a small scaling factor to tune the oscillation position and amplitude to the values observed in the experiment.

The second moments (variances) are evaluated from a similar relation according to the definition in equation (7). The evaluation of the spectral moments according to the above model will be assigned in the following as *continuum* approximation.

The described model holds only for not too small values of $\sigma$. A reasonable limit is $\sigma \geq a_{\rm CC}/3$ which corresponds to the smallest width of the integration interval ($\pm a_{\rm CC}/6$ for $j = 1$).

### 2.4 Comparison between full DOS and continuum calculation

To check the difference between full DOS and continuum calculation an evaluation of the spectral moments was performed for a typical tube with mean diameter of 1.36 nm and variance $\sigma^2 = 0.01$. The full DOS calculation yields a damped oscillation *versus* excitation energy for the first and for the second moment. This is demonstrated in Figure 1a. The noise in the result originates from the singularities in the density of states. Up to 4 oscillations can be detected before the latter are damped out for excitation in the blue and ultraviolet spectral range. To obtain the results as plotted the energy scale was up-shifted by 10% and then continuously chirped to obtain un-scaled energies from 1.6 eV upwards. This process is necessary to compensate for the influence of $g_j$ in the approximate evaluation of the moments according to equation (8). As it will be discussed below this rescaling of the tight binding transition energies is an intrinsic property of the response.

The dashed line in the figure represents the result from the continuum approximation according to equation (8). For the first moment the agreement between full DOS and approximate calculation is very good except that the latter yields a too large amplitude for the first oscillation. For the variance the agreement is almost as good except that for the approximation the first oscillations appear too sharp and too strong. In both cases the response evaluated for the variance is phase shifted by $\pi/4$ as compared

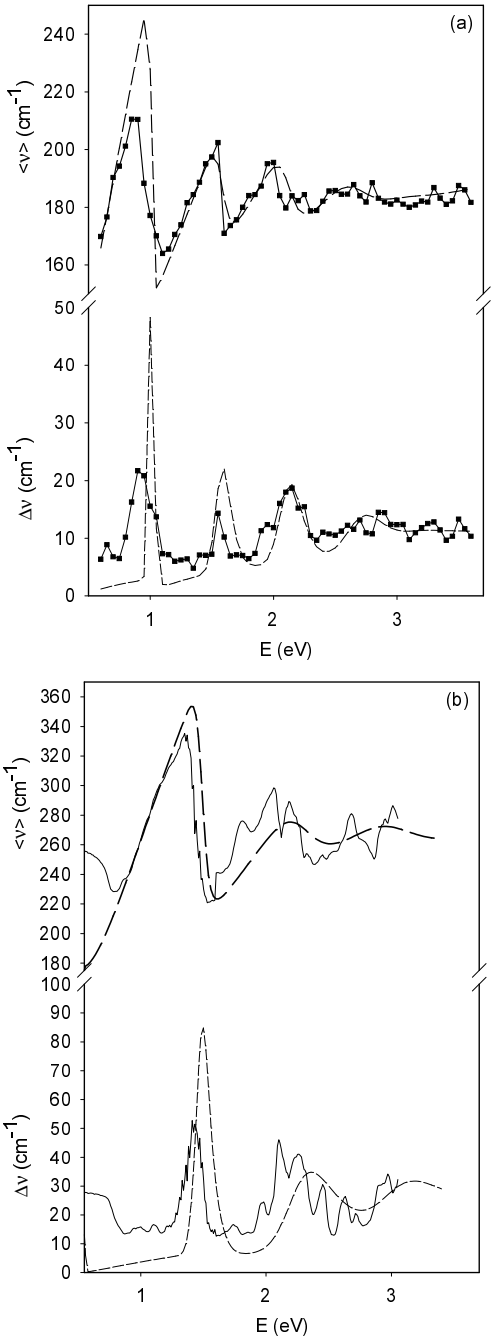


**Fig. 1.** Comparison between calculated first and second moments using the DOS explicitly (full squares) and continuum approximation (dashed line). $C_2 = 9.5$ was assumed in both cases. For the full DOS calculation a phonon line width $\Gamma = 2$ cm$^{-1}$ was used. (a) for a distribution with $d_0 = 1.36, \sigma_0 = 0.1$, (b) for a distribution with $d_0 = 0.9, \sigma_0 = 0.1$.

to the first moment. Also, it is important to note that both, the first moments and the variances are characterized by their absolute value, their oscillation frequency and shape, their oscillation amplitude, their oscillation phase and by their damping. It means all these quantities are relevant parameters to be determined in an experiment.

Figure 1b presents the same comparison but for tubes with 0.9 nm diameter. Obviously the agreement is not as good, particularly for low energies. The peaks from the continuum approximation appear up shifted as compared to the full DOS calculation. Only for energies higher than about 2.3 eV both models yield the same result within an expected experimental error. Thus, as a rough estimate, for diameters down to 1 nm the approximate model is reliable for the whole spectral range whereas for smaller tubes analysis must be limited either to energies larger 2.3 eV or the full DOS evaluation must be used.

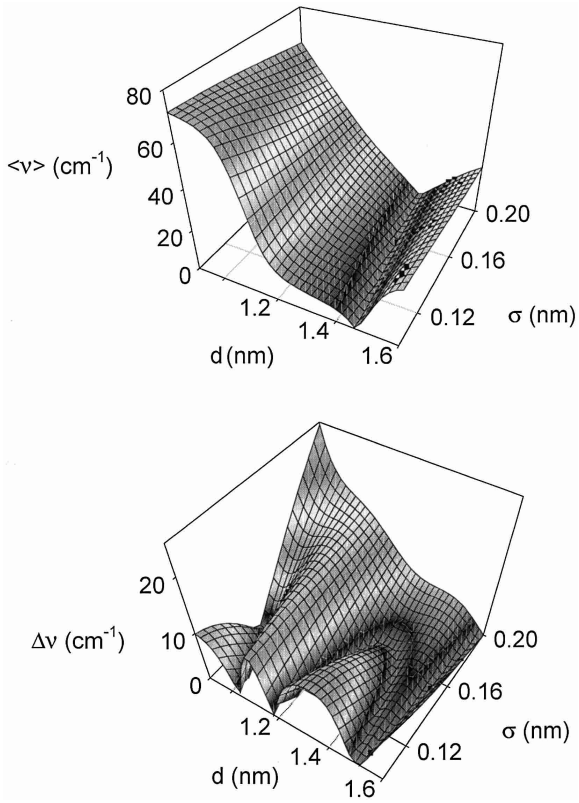


**Fig. 2.** Reduced first moment $\langle\nu\rangle = \langle\nu(d,\sigma)\rangle - \langle\nu(d_0,\sigma_0)\rangle$ (a) and reduced variance $\Delta\nu = \Delta\nu(d,\sigma) - \Delta\nu(d_0,\sigma_0)$ (b) as a function of $d$ and $\sigma$ for a distribution with $d_0 = 1.36$ nm and $\sigma = 0.16$ nm.

### 2.5 Evaluation of diameters and diameter distributions

For the evaluation of $d_0$ and $\sigma$ equations (7) and (8) must be solved simultaneously. Since these equations are highly nonlinear solubility can be expected if the two equations depend strongly on $d$ and $\sigma$. This dependence can be checked by studying the two quantities as a function of $d$ and $\sigma$ for a known distribution with parameters $d_0$ and $\sigma_0$. Figure 2 depicts this response for a particular laser excitation of 1.92 eV in a two-dimensional graph for a distribution with $d_0 = 1.36$ nm and $\sigma_0 = 0.16$. The values on the $z$-axis represent the evaluated response reduced by the moments valid for the distribution under consideration. Thus, the ditch for zero or minimum response represents the correct solution for $d$ and $\sigma$ in both cases. Since the ditch is well expressed a unique solution can be expected

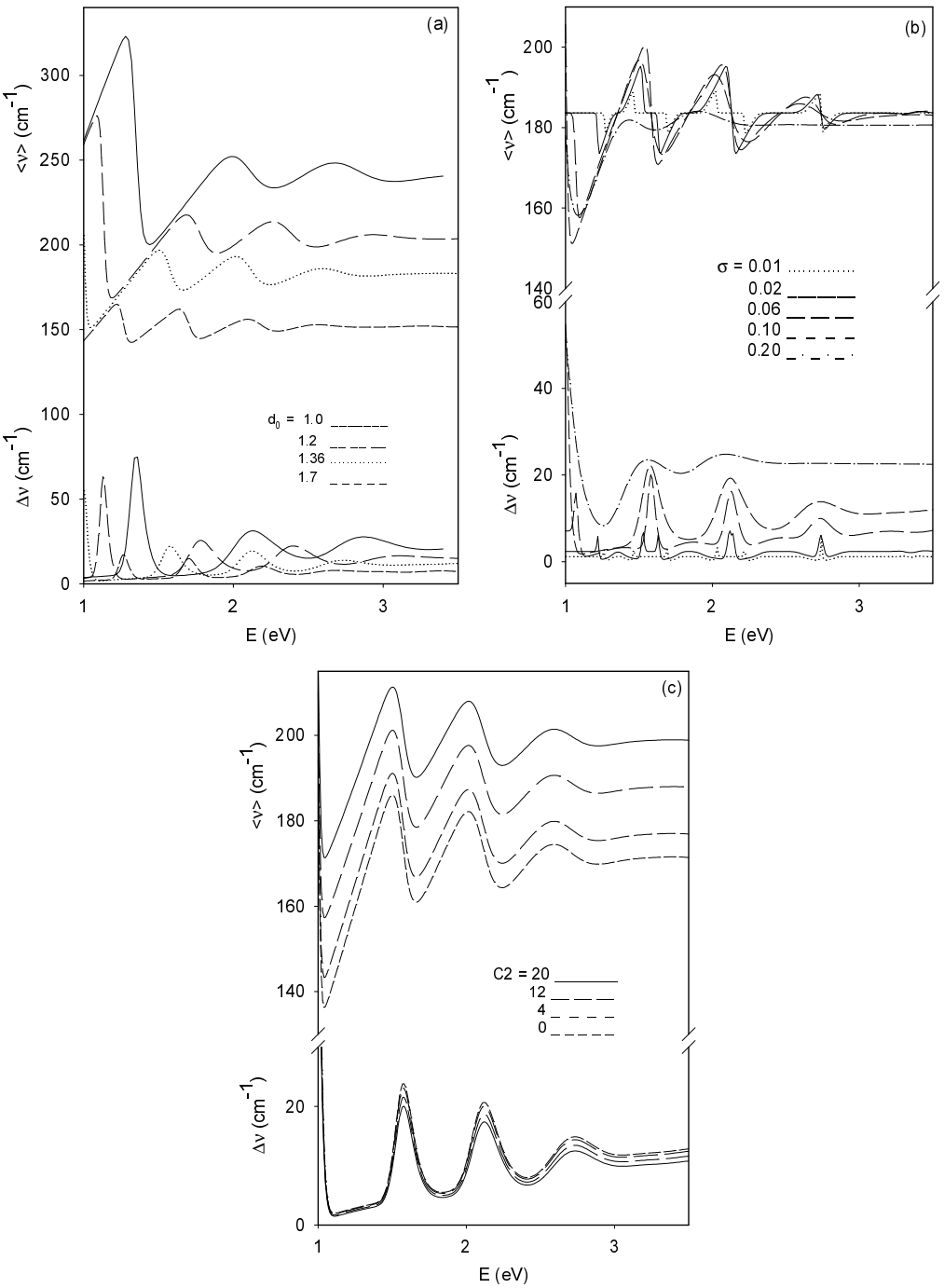


**Fig. 3.** First moments and variance for the Raman response of the radial breathing mode *versus* energy of the exciting laser for different parameters of the distribution. (a) different values of $d_0$ as indicated; $\sigma = 0.1$, $C_2 = 9.5$ cm$^{-1}$. (b) different values of $\sigma$ as indicated; $d_0 = 1.36$ nm. $C_2 = 9.5$ cm$^{-1}$. (c) different values of $C_2$ as indicated. $d_0 = 1.36$, $\sigma = 0.1$.

for this sample. Similar graphs can be obtained for other laser energies. The ditch becomes rather flat for excitation with low energy lasers.

As a summary from the analyzes carried out on the various samples described below in 90% of all trials the system of the two equation was soluble by *Mathematica*. Lack of convergence for the solution was only encountered for the tube material with the smallest diameter and for excitation with deep red laser light.

## 3 Response to the parameters of the diameter distribution

In order to use the above model for the analysis of SWCNT material it is necessary to study its response to a wide range of parameters. Results for excitation with a continuous distribution of laser energies are depicted in Figure 3. Part (a) exhibits the oscillations of the first moment for different diameters between 1 and 1.7 nm. As expected the

mean value shifts upwards with decreasing mean diameter $d_0$. In addition there is a phase shift of the oscillations. The positions of the first, second, third, etc. maxima shift to higher laser energies with decreasing tube diameter. For very small tubes a new peak enters on the low energy side. From the position of the peaks for the tube with diameter 1.36 nm (dotted line) we can formally correlate the first, second and third peak with the second and third transition of semiconducting tubes and with the first transition of metallic tubes, respectively. Interestingly the oscillations become rather flat for excitation energies above 2.5 eV, almost independent from the tube diameter. For excitation with the Nd:YAG laser (1.17 eV) the response even from the first transitions in semiconducting tubes becomes relevant for small tubes and exhibits a giant oscillation of 120 $cm^{-1}$. Similarly, the variance becomes very large for this laser. On the other hand the discrimination between tubes with different diameters in the range of 1.2 to 1.7 nm becomes difficult whereas the discrimination of tubes with smaller diameter is easy. In fact from the graph one expects a discontinuity of the mean value of the RBM frequency for tubes around than 1 and 1.2 nm. This is indeed observed in the experiments as shown in Section 5.

Figure 3b depicts a similar set of response curves for constant tube diameters but varying second moment. As one might have expected the oscillations smear out for broad distributions but they also decrease for very narrow distributions. In the latter case the peaks in the variance split into two components.

Finally, Figure 3c exhibits the response to $C_2$ which characterizes the intertube interaction. The up shift of the response with increasing intertube interaction is natural but it occurs without phase shift. This is in contrast to the shift originating from decreasing diameter. It means that the up shift of the RBM frequencies as a consequence of decreasing tube diameter and as a consequence of increasing intertube interaction can be discriminated in the evaluation.

The quenching of the oscillations for narrow distributions becomes only significant for values of $\sigma \leq 0.05$ nm. The evaluation of this behavior can not be obtained straight forwardly from equation (8) since this equation holds only for $\sigma \geq a_{CC}/3$ as already mentioned above. For smaller values of $\sigma$ contributions from the energy region between the van Hove singularities can not be neglected. A formal extension of the formula as depicted in the Appendix allows, however, to include very narrow distributions in the analysis. The resulting amplitudes of the oscillations are shown in Figure 4 for two different mean values of the tube diameters.

The above analysis indicates that the determination of the mean tube diameter from the first moments needs some care. The $1/d$ law may not be valid under certain conditions. Figure 5 gives an example. The dashed line represents the $1/d$ law. The two full drawn lines represent the connection between the observed first moments for a particular distribution characterized by $1/d_0$ and two different excitation energies. For the IR excitation the deviations from the $1/d$ law are dramatic but even for the green laser excitation measurable deviations occur. A difference between $1/d_0 = 0.65$ and $1/d_0 = 0.7$ is significant in the experiment.

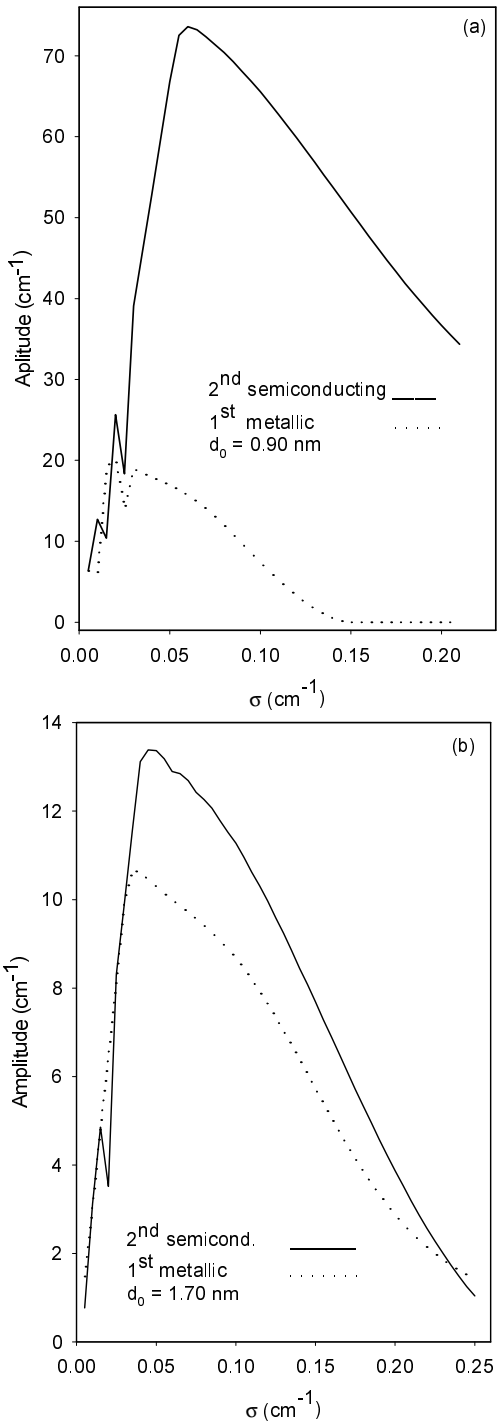


**Fig. 4.** Values for the second and the third peak to minimum amplitude of the oscillations in Figure 3 *versus* width of the distribution. (a) mean diameter $d_0 = 0.9$ nm, (b) mean diameter $d_0 = 1.7$ nm. $C_2 = 9.5$ $cm^{-1}$ was used in both cases. The third peak in the oscillations in Figure 3 originates from the first van Hove singularities in metallic tubes.

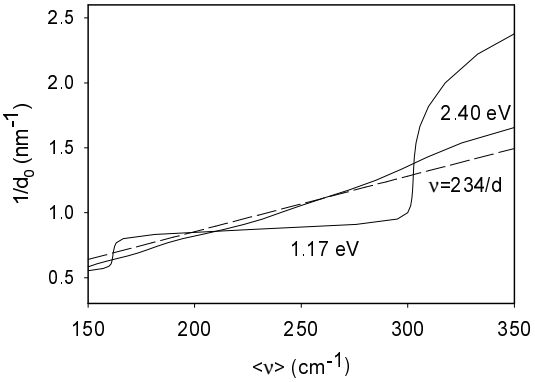


**Fig. 5.** Inverse of average tube diameters in $nm^{-1}$ *versus* first spectral moment for a Gaussian distributions with $\sigma = 0.15$ nm. Excitation energies are as indicated. The dashed line represents $1/d = \langle\nu\rangle/234$.

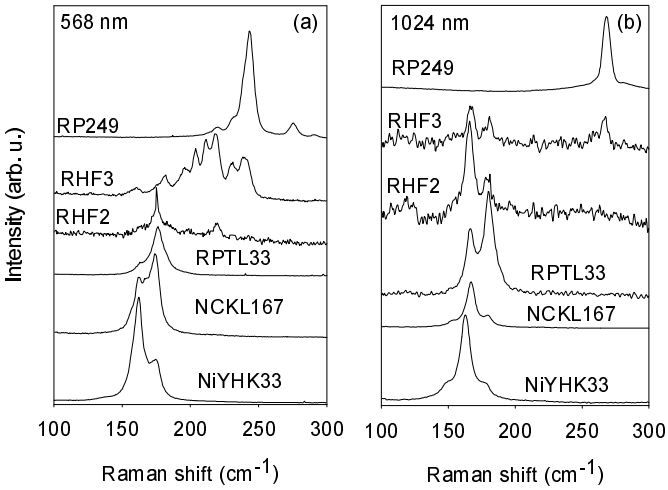


**Fig. 6.** Raman response of the RBM for 6 different samples; (a) as excited with a yellow laser at 568 nm and (b) with an IR laser at 1064 nm (b).

## 4 Experimental

SWCNTs with 6 different mean diameters were prepared by arc discharge and laser ablation as described previously in detail [12,13]. The diameters estimated from previous Raman and X-ray analyzes extended from 0.9 nm to 1.7 nm. The samples were suspended in toluene and then drop-coated to form a thick film on a hot silicon substrate (for the Raman and X-ray experiments) or drop-coated on a hot quartz substrate to form a thin film for the optical transmission experiments. The obtained films were annealed at 1000° in high vacuum for 12 hours and then slowly cooled to room temperature. Raman spectra were recorded in the spectral range of the RBM with 7 different laser lines extending from 454 nm to 1064 nm (1.17–2.73 eV) for all samples. For two selected samples (smallest and largest diameter) a full set of 30 laser lines was used for the excitation. The spectral resolution was 2 $cm^{-1}$ and the measurements were taken at a room temperature. Analysis and detection of the scattered light was performed with a Dilor xy spectrometer and a liquid nitrogen cooled CCD detector. The system was calibrated for intensities by recording the resonance cross section of the $F_{1g}$ mode of Si.

Optical transmission was studied for the thin films on quartz with a Hitachi U3410 spectrometer in the spectral range between 0.7 and 5 eV with a spectral resolution of 20 meV.

In order to control the analysis from Raman and optical experiments X-ray diffraction was recorded for all samples. $CuK_\alpha$ from a rotating anode was used together with a pinhole camera and a 2D position sensitive detector [25] for scattering vectors between 2 and 18 $nm^{-1}$.

## 5 Results

### 5.1 Raman response of the RBM for selected lasers

As expected from many previous experiments the response for excitation with different lasers revealed very rich and strongly differing spectra for each sample. Figure 6 depicts two examples, one for excitation with a yellow laser and one for excitation with the IR laser. In the latter case the discontinuous jump of the position of the RBM with changing diameter for small tubes is obvious. In contrast to this there is very little change on the mean line position for larger tube diameters. This is exactly as predicted from Figure 3a. Also, since the shape and width of the spectra in part (a) of the figure exhibit strong variations they can not reflect directly the width of the diameter distribution.

A straight forward analysis of the average positions of the RBM for the 7 laser lines yields a fluctuation up to 30 $cm^{-1}$ for the first moment evaluated for one and the same sample and a corresponding high uncertainty in the average tube diameter of 15%. In contrast, applying the above described formalism the diameter of the tubes could be determined with a much smaller experimental error which eventually turned out to be of the order of 2%.

The analysis was performed in general by determining $d_0$ and $\sigma$ for a constant value of $C_2 = 9.5$ in a first approximation. A fine tuning was obtained by calculating the moments for the obtained values of $d_0$ and $\sigma$ and fitting the oscillations to the experimental points with $C_2$ as a fitting parameter. The resulting curves touched the experimental points very well. A comparison between experiment and calculation is depicted in Figures 7a, b for two different samples. The figure clearly demonstrates the importance of using the oscillatory model. With the new values for $C_2$ new values for $d_0$ and $\sigma$ were retained. In general the applied fitting cycle had only little influence on the results for $d_0$ and $\sigma$ but revealed variations in $C_2$. The final values for $d_0, \sigma$, and $C_2$ are collected in Table 1 for the 6 samples, together with the root mean square error for $d_0$.

**Table 1.** Diameters and diameter distributions for single wall carbon nanotubes. $N$ is the number of tubes per bundle as determined from equation (13) in combination with equation (14) and for $c = 0.7$. $D$ is the bundle diameter in nm.

| Sample | Tube diameter (Raman) [nm] | Distribution width $\sigma$ (Raman) [nm] | Intertube shift $C_2$ and $(N, D)$ (Raman) [cm$^{-1}$] | Tube diameter (X-ray) [nm] | Coherence length (width $\sigma$) (X-ray) [nm]([nm]) | Tube diameter (optics) [nm] | Distribution width $\sigma$ (optics) [nm] |
|---|---|---|---|---|---|---|---|
| RP249 | 0.94±0.02 | 0.11±0.04 | 14 (8.2,5) | 0.97 | 20 (-) | 0.94 | 0.13 |
| RHF3 | 1.17±0.04 | 0.14 ±0.03 | 9 (3) | 1.16 | 25 (0.2) | 1.18 | 0.16 |
| RHF2 | 1.30 ±0.02 | 0.14 ±0.02 | 11 (4) | 1.24 | 25 (0.18) | 1.29 | 0.11 |
| NCKL167 | 1.39 ±0.01 | 0.15±0.03 | 16 (10,7) | 1.35 | 50 (0.07) | 1.38 | 0.11 |
| RPTL33 | 1.47 ±0.02 | 0.14 ±0.02 | 18 (20,10) | 1.40 | 10 (0.18) | 1.41 | 0.12 |
| NiYHK33 | 1.53±0.02 | 0.14 ±0.04 | 20 (44,15) | 1.48 | 25 (0.16) | 1.47 | 0.12 |

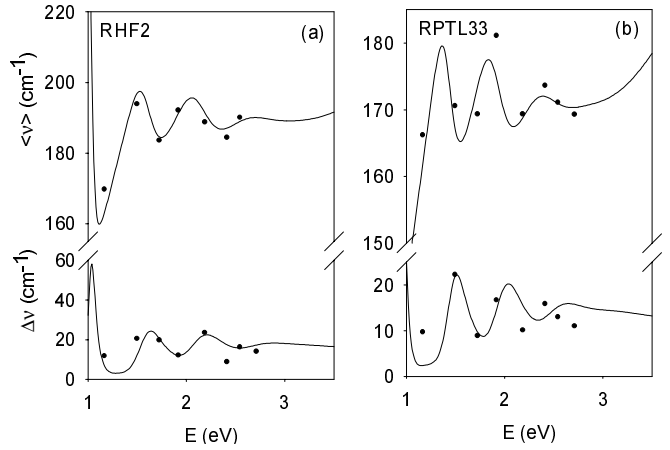


**Fig. 7.** Experimentally evaluated first moments and variances for two different nanotube samples; (a) RHF2 with mean diameter $d_0 = 1.30$ nm, $\sigma = 0.14$ nm, $C_2 = 11$ cm$^{-1}$ and (b) RPTL33 with mean diameter $d_0 = 1.47$ nm, $\sigma = 0.14$ nm $C_2 = 18$ cm$^{-1}$. Full drawn lines are from the continuum approximation.

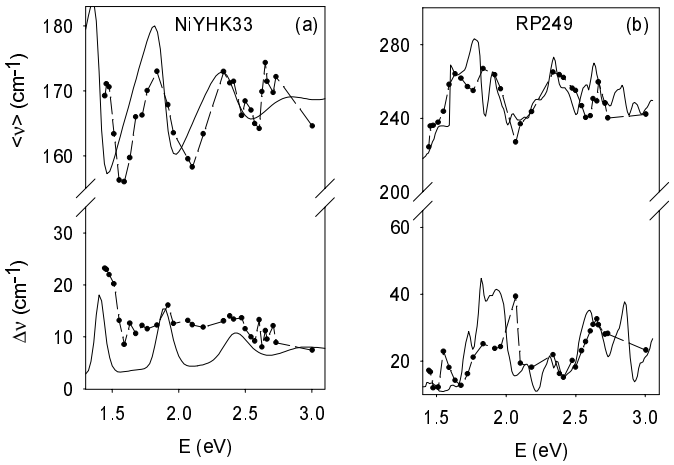


**Fig. 8.** Same presentation as in Figure 7 but for 30 different laser lines: (a) sample NiYHK33 with mean diameter $d_0 = 1.53$ nm, $\sigma = 0.14$ nm, and (b) sample RP249 with mean diameter $d_0 = 0.94$ nm, $\sigma = 0.1$ nm. The full drawn line in (b) is obtained from the full DOS calculation with $\gamma_0 = 2.55$ eV.

### 5.2 Samples with very large and very small diameter

For the samples with largest (NiYHK33) and smallest (RP249) diameter a full set of 30 laser lines was used to determine the spectral moments. Results are depicted in Figure 8. For the sample with large diameter four oscillations waves can be seen. The continuum approximation fits the four oscillations from the experiment well even though the oscillation frequency appears a bit too large. Since in this case as well as for the sample RP249 a large enough number of experimental data was available a direct fit of the experimental results to the first moments was performed in addition. Fitting parameters were simultaneously $d_0$, and $C_2$. In the case of NiYHK33 results for $d_0$ were about 4% smaller than those from solving the two equations (7) and (8). With the smaller values for $d_0$ the agreement between experiment and calculation improves.

For sample RP249 the smallest diameter of only 0.94 nm was observed but only laser energies larger than 2 eV could be used for the evaluation. Also, plotting the first moments *versus* laser energy for the continuum approximation as well as for the full DOS calculation revealed noticeable disagreement between experiment and calculation. This discrepancy could only be avoided by re-fitting the experimental data and including $\gamma_0$ as a fitting parameter. Very good agreement was then obtained with a value for $\gamma_0 = 2.55$, particularly for the full DOS calculation. Data from this fit are depicted in Table 1.

A comparison between experimental results and calculation is depicted in Figure 8 for the two samples. Note that in the case of the sample with the small tube diameters the full DOS calculation was applied to evaluate the theoretical curve.

### 5.3 Results from optical absorption

Optical absorption has been used as an alternative tool to determine SWCNT diameters [11,12]. It was therefore important to compare results form this technique with the results from Raman experiments. After recording the spectra for all 6 samples the overall background was subtracted and the well known absorption peaks for the first and second transition for semiconducting tubes and the first transition for metallic tubes were observed. These spectra are

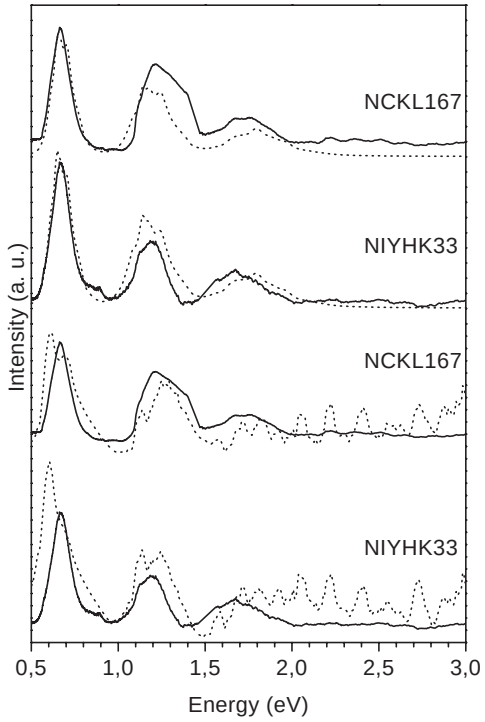


**Fig. 9.** Optical absorption for two different SWCNT samples as indicated and after subtraction of the background (full line). Calculated absorption spectra are shown as dashed lines. The upper two dashed spectra hold for a calculation using the full set of DOS functions. The lower two dashed spectra hold for the approximation according to equation (11).

very similar to the absorption spectra reported by Kataura *et al.* in [12]. The two higher absorption peaks exhibited a fine structure as it was also reported before [11]. Results for two selected samples are depicted in Figure 9 as full drawn lines.

To obtain the parameters for the diameter distribution from the experiment one can proceed as in the case of the Raman experiments. The full set of DOS functions can be supper imposed to represent the quasi-continuous distribution of nanotubes. Each tube is again weighted with a Gaussian factor. Assuming constant matrix elements like in the case of the Raman analysis the absorption is obtained from

$$\alpha(\epsilon) \propto \sum_{m,n} \exp\left[-\frac{(d_{n,m}-d_0)^2}{2\sigma^2}\right] g^2_{n,m}(\epsilon). \qquad (10)$$

Subtracting again the background renders characteristic peaks for the optical transitions between the van Hove singularities. Using the same value of $\gamma_0 = 2.9$ eV for the $\pi$-$\pi$ overlap and a similar up scaling for the first two transitions as it was applied in the case of the Raman analysis one can fit $d_0$ and $\sigma$ to the experiments. Corresponding results are depicted for the two tube materials as dashed lines in the upper part of Figure 9. The calculated spectra were obtained for $d_0 = 1.38$ nm, $\sigma = 0.11$ nm (NCKL167) and $d_0 = 1.47$ nm, $\sigma = 0.12$ nm (NiYHK33), respectively, in very good agreement with the results from the Raman experiments. The agreement is not only good with respect to line position but also with respect to line width and intensity. Similar good agreement was obtained for the other samples. For the smallest tube PR249 again the value for $\gamma_0$ had to be reduced to yield best agreement with the experiment.

The fine structure in the second and third peak of the calculated spectra is retained with a very similar shape as observed in the experiment. Thus, similar to the Raman spectra it is not smeared out by the overlap from the large number of tubes considered.

The alternate possibility for the analysis of the optical spectra is to apply an approximation where only the density of geometrically allowed tubes is considered weighted with the Gaussian probability for each tube.

$$\alpha(\epsilon) \propto \sum_{m,n,j} \exp\left[-\frac{(d_{n,m}-d_0)^2}{2\sigma^2}\right] \times \frac{\delta}{(\epsilon-\epsilon_j(n,m))^2+(\delta/2)^2}\cdot \qquad (11)$$

$\delta$ is a small value of the order of 10 meV describing the finite resolution of the spectrometer and the width of the resonant electronic states $j$ due to lifetime effects. $\epsilon_j(n,m) = 2jg_j a_{CC}\gamma_0/d(n,m)$ is the same quantity as used in equation (8). This means the evaluation is performed in direct analogy to the continuum approximation of the Raman data. Experimental results can be fitted again by varying $d_0$ and $\sigma$. In the lower part of Figure 9 results are depicted for the same two samples as selected in the upper part. Agreement with the experiment is even better than for the full DOS calculation. Similar good agreement was obtained for the other samples. Results for $d_0$ and $\sigma$ are listed in Table 1.

### 5.4 Results from X-ray diffraction

The traditional method to determine diameters of SWCNTs is X-ray diffraction. The diffraction pattern of large bundles provides insight into the lattice constant of the hexagonal lattice and can thus give information on the tube diameter, coherence length (coherent bundle diameter) and diameter distribution. Evaluation of all these data is only possible if samples are of high quality as it needs to consider several of the small side bands accompanying the main diffraction peak from the hexagonal lattice at a scattering vector $q = 4.3$ nm$^{-1}$. All samples revealed reasonably good peaks which enabled a detailed analysis, except for the material with the smallest tube diameters. For this material, due to the high background, only one peak could be identified. The position of the maximum was used to calculate the tube-tube distance and the tube diameter by subtracting the Van der Waals distance. In the raw data a strong increase in scattering intensity can always be observed for small $q$. This small-angle scattering originates from large objects and has to be subtracted by an appropriate procedure [5,7]. Figure 10 depicts an example for sample NCKL167 after this background correction. Details of the subtraction procedure as well as details

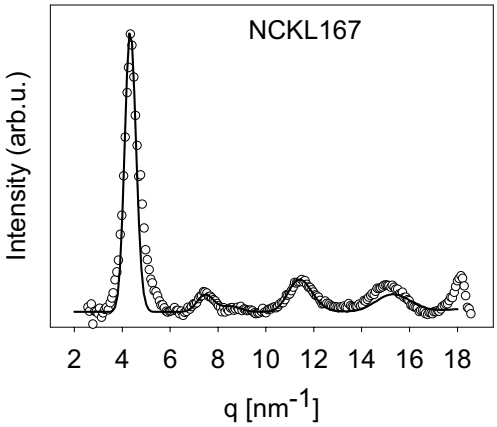


**Fig. 10.** X-ray diffraction intensity after appropriate subtraction of the background (circles). The line is a fit from the diffraction model. The disagreement between experiment and fit for the fourth peak is due to model simplifications. The fifth peak at 18 $nm^{-1}$ originates from graphitic carbon.

for the following analysis will be described elsewhere [26]. The four diffraction peaks between 4 and 16 $nm^{-1}$ originate from the nanotubes in the bundles.

The model used for the evaluation of the diffraction spectra is based on the following assumptions: The tubes exhibit an outer radius $r_1$, an inner radius $r_2$ and thus a wall thickness $w = r_1 - r_2$. They are of infinite length, arranged in a perfect hexagonal lattice and diameters are subjected to a Gaussian distribution. The mean tube diameter $d_0 = r_1 + r_2$. The intensity of the Bragg reflections was calculated by using the model for random layer lattices [28]. The average intensity of the Debye-Scherrer rings is then proportional to the following equation, excluding constants but including the polarization factor and the Lorentz factor for 2D layer lattices.

$$I(\theta) \propto \frac{\cos\theta(1+\cos^2 2\theta)}{\sqrt{\sin\theta}} \times G\left(\frac{2L\sqrt{\pi}}{\lambda}(\sin\theta - \sin\theta_0)\right) F^2(q(\theta)), \quad (12)$$

with

$$G(a) = \int_0^\infty \mathrm{d}x \exp[-(x^2 - a)^2].$$

$F$ is the form factor, $L$ the particle dimension and $\theta_0$ the respective Bragg reflection angle. A Debye-Waller factor was neglected, as for carbon the intensity reduction in the whole observed $q$-range is below 2%. The form factor for a cylinder is given by the Bessel-function of the first order [29] and has the form $F^2(q) \propto [r_1 \mathrm{J}_1(q, r_1)/(qr_1)]^2/q$. The diffraction from the tube can be evaluated from the absolute value of the subtraction of two cylinders, one with the outer and the other with the inner radius of the tube. The model is similar to the one described by Rols *et al.* [7], but is based on the model of layer lattices [27]. Thus, all peaks can be used for a quantitative description, whereas the intensities for the higher order peaks were weaker in the experiments than predicted by the model of Rols [7]. The tube thickness was fixed to 0.08 nm to reduce the number of free parameters. This value is consistent with a nanotube of only one wall. The resolution function of the spectrometer was measured by crystalline powder and used for modeling the width of the peaks. An additional broadening was simulated by assuming a distribution of tube diameters which leads to an increased peak width for the higher Bragg reflections and is similar to a lattice distortion. The model with the tube diameter, the tube distance, the diameter distribution and the crystal size as four parameters is then fitted to the experimental results.

The first peak determines the center to center distance of the tubes and can be measured with high precision. The absence of the (2 0), (3 0) and (4 0) reflections along the $q$-axis is the most remarkable point and gives a strong restriction to the form factor, *i.e.* it determines the tube diameter. The width of the higher reflection peaks increases which is attributed to the size distribution of tube diameters. In the model, due to geometric restrictions larger tube diameters cause larger tube distances, *i.e.* the Van der Waals distance is assumed to be a constant. This suggests that within the bundles regions with larger and smaller tube diameters coexist. A description by using a mean tube diameter and a mean tube distance, which would be the consequence if tubes of different size are completely mixed, does not adequately reproduce the experimental results. This interpretation is particularly reliable for specimen NCKL167, where the narrow diameter distribution permits such a refined evaluation.

The peak at 18 $nm^{-1}$ originates from the (002) reflection of graphite. Its small width which is even smaller than the width of the first nanotube reflection, and the pronounced asymmetry towards small q is typically for highly oriented (turbostratic) graphitic carbon [28]. As the area of the graphitic peak is significantly smaller than the one of the nanotubes, it can be concluded that the amount of graphitic carbon is significantly smaller than the one which formed the nanotubes. There exists an additional part of amorphous carbon in the specimen, which could not be determined, since the background from small-angle scattering and from amorphous carbon cannot be distinguished with sufficient precision.

The results obtained from the evaluation are shown in Table 1, columns 5 and 6. Precise values are obtained for the diameter and the distance (diameter plus Van der Waals distance) of the tubes. The differences between fit and experimental results in the wings of the first peak may be attributed to a non-Gaussian distribution of the tube diameters. This could lead to a small overestimation of the fit parameter for $\sigma$ of the tube diameter distribution. As the parameter $L$ only slightly influences the fit the determination of the crystal size is not very accurate.

## 6 Discussion

The two models developed in this work are the basis for the analysis of the tube material. Both models have their

merits. The continuum model is easier to handle and allows a direct analysis of tube diameters, even if only a small number of laser lines have been used for the excitation of the spectra. In the extreme case of small tubes or very narrow diameter distributions it suffers from over simplification. The full DOS model is more elaborate but holds also for thin tubes. The reduced value of $\gamma_0$ for small tubes is really surprising. From hand waving arguments one would rather expect a further increase of the $\pi$-$\pi$ overlap with increasing curvature of the tubes. On the other hand it is known that $\sigma$ orbitals increasingly contribute to the electronic structure of the $\pi$ system [30] which may indeed change the electronic response and has some influence on the van Hove pattern.

The need for the increase of the transition energies between the first two van Hove singularities must be considered as intrinsic as it holds for the evaluation of the Raman data as well as for the evaluation of the optical spectra. It is most probably due to the shortcomings of the tight binding approximation which was used for the evaluation of the band structure (Eq. (2)). In a recent theoretical analysis by Ando *et al.* [31] it was demonstrated that the Coulomb interaction between the electrons in the $\pi$-band leads to exciton levels and to an up shift of the transition energies between the van Hove singularities. This up shift is particularly strong for the lowest energy transition and can reach 20% for a Coulomb interaction of the order of 0.1 eV. This upshift was observed recently from a mismatch between experimentally observed absorption and results from tight binding calculations [32].

### 6.1 Quantum oscillation and diameter distribution

The presented models can explain several unexpected experimental results. One of them is the oscillation of the spectral moments which are identified as a quantum size effect originating from the small dimension in radial direction. The laser energy is swept across the van Hove singularities and excites oscillating tube diameters to resonance. Other unexpected results are the discontinuous switch of line position for the RBM mode with changing tube diameter if the excitation is performed with red or IR light. Oscillations are well expressed for such excitations whereas for the determination of diameter distributions blue or green lasers are recommended.

For the Raman as well as for the optical and X-ray analysis the size of the probe extends over several thousand bundles. Therefore the obtained diameter distributions should be representative in all three cases. Indeed, the results from the Raman experiments are in excellent agreement with results from optics and X-rays. The experimental error for $d_0$ given in Table 1 is a real root mean square error obtained for the excitation with the various lasers. The error for $\sigma$ is of the same relative magnitude. X-ray analysis yields very reliable data for tube diameters but more details suffer from the strong background which has to be subtracted. Better samples and even more refined analyzes might help.

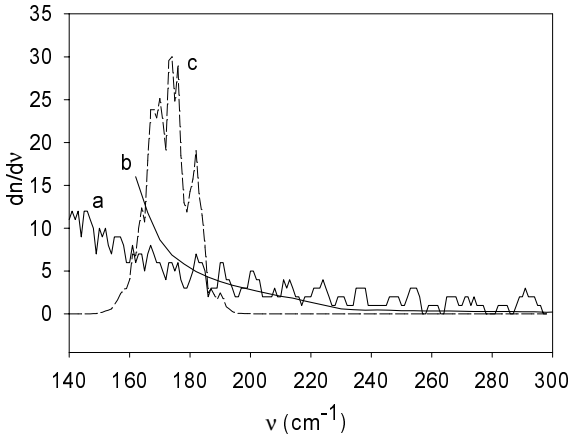


**Fig. 11.** Clustering in the distribution of tube diameters for small SWCNTs and origin of fine structure in the Raman line for the RBM; *a* density of RBM frequencies *versus* RBM frequency (or tube diameter); a sampling width of 3 $cm^{-1}$ was applied; *b* same plot as *a* but for large tubes. (The left hand side of the line corresponds to 10 nm diameter or 23.4 $cm^{-1}$.) The whole curve was shifted onto the top of curve *a* by scaling the *x*-axis and *y*-axis to provide immediate comparison. *c* as curve *a* but each tube was weighted with its probability in a Gaussian distribution of diameters.

Both, the Raman results and the optical spectra reveal a fine structure which needs some more discussion.

### 6.2 Origin of the fine structure

In previous work and in the current presentation we have demonstrated that the full DOS model as well as the continuum approximation provide a good representation for the fine structure in the Raman spectra of the RBM and in the optical absorption spectra. This is still surprising since the response originates from an overlap of a rather large number of tubes with only slightly varying properties. The physical reason for the fine structure can be traced back in fact to the nanoscopic geometry of the tubes. For such small entities the distribution of tube diameters is not really quasicontinuous but exhibits clusters. This is demonstrated in Figure 11. The figure shows the density of diameters or, more precisely, the density of RBM frequencies for a certain frequency interval for two selected ranges of tube diameters. For the small tube as they are usually prepared in nanotube research clustering is evident (curve *a*). For large tubes (which have not been prepared so far as single wall species) the density *versus* frequency relation is completely smooth (curve *b*). If we weight curve *a* with a Gaussian distribution we obtain curve *c* which is almost a representative for the fine structure in the Raman response of the RBM.

The clustering of the RBM frequencies is related to the clustering of the diameters and the latter correlates immediately to the clustering of resonance transitions. This means there is a clustering of resonance cross sections which certainly further enhances the development of a fine structure.

### 6.3 Bundle diameters and intertube interaction

The stiffening of the RBM frequency by the intertube interaction was demonstrated by us already in previous work [8,17]. This effect is fully confirmed here for tubes with different diameters. The requested up shift of the frequencies calculated for individual tubes is determined by the function $C_2$. This function was found by Henrard *et al.* [23] to depend on the tube diameter. Evaluating their data explicitly yields a relation of the form

$$C_2(d) = \frac{(10.3d - 2.3)2.56}{d} \cdot \tag{13}$$

In a recent paper by Henrard *et al.* [22] it was demonstrated that $C_2$ depends not only on the tube diameter but also on the number of tubes in the bundle, at least as long as the bundles are not too big. Up to about 100 tubes per bundle can give a selective response. In this case the value of $C_2$ can provide information on the bundle diameter. The final shift of the RBM mode for infinite large bundles increases about linearly with the tube diameter. Considering this findings one can use the following refined formula for the evaluation of the number of tubes in the bundle.

$$\begin{aligned} C_2'(N,d) &= cC_2(d)a(N) \\ &= \frac{c(10.3d - 2.3)2.56}{d}\left(1 - \frac{1}{N^{0.46}}\right) \cdot \end{aligned} \tag{14}$$

$c$ is a scaling factor describing the tube-tube interaction in the bundles ($c = 1$ for the work of Henrard *et al.*) explicitly and $a(N)$ is a function describing the behavior for small numbers of tubes in the bundle. $a(N)$ was determined from a best fit to the relation calculated in reference [22]. The fit and a set of relations according to equation (14) are depicted in Figure 12 for different tube diameters. Using the values for the intertube interaction for infinitely large tubes from the calculation in reference [23] the resulting shifts are much larger than the observed up shifts. This would require very few tubes per bundle in contrast to various other measurements. The intertube interaction calculated in reference [21] is about 30% smaller and yields more realistic results in the present case. Even for this reduced interaction potential the limiting case for the stiffening is not reached. Therefore equation (14) could be solved for $N$ for all tubes under investigation using the observed up shifts. The resulting values for $C_2$ and $N$ are depicted in Table 1 in column four. From the values obtained for $N$ the bundle diameter can be evaluated from

$$D = (d + 0.6)\sqrt{\frac{2\sqrt{3}N}{\pi}} \tag{15}$$

for a hexagonal arrangement of the tubes. This yields for the four largest bundles from Table 1: 15, 10, 7, and 5 nm, respectively. The evaluated diameters for the bundles are of course only as good as the calculation. A more rapid saturation for the up shift of the RBM frequency with bundle diameter was found by Popov *et al.* [33]. In this case bundle diameters would be even smaller. A weaker interaction would yield larger bundles.

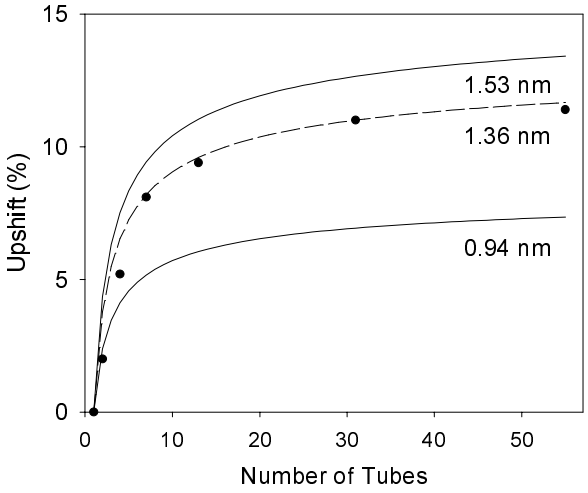


**Fig. 12.** Relative shift of the RBM frequency in SWCNT bundles as a consequence of intertube interaction. Bullets are as calculated from reference [22]. The dashed line is a best fit using equation (14). The full drawn lines hold for $d_0$ as indicated.

Certainly also the constant of 234 cm$^{-1}$ nm is crucial for the evaluation. A smaller value would result in a stronger up shift from the tube-tube interaction. Higher values would reduce the number of tubes in the bundles. However, as the *ab initio* calculations from reference [20] must be considered as very accurate there is little room for adjustment from this side.

The coherence lengths from X-ray might be a comparative quantity to the evaluated bundle diameters. From Table 1 they turn out much larger than the diameters evaluated from Raman. This is not really surprising. X-rays sees only the large bundles but never an individual tube or bundles with two or three tubes. In contrast, Raman scattering records all tubes, no matter how small the bundles are to which they belong. This makes certainly a difference.

## 7 Summary

Raman scattering and in particular the response from the RBM has again proven to be an excellent tool for the analysis of SWCNTs. However, to draw the full information buried in this response a careful analysis is requested. The oscillations in the frequency response could be traced back to the size quantization of the tubes in transversal direction. The evaluation of the first and second spectral moment of the radial breathing mode response allows to determine tube diameters and, if the bundle size is not in the limit of infinite large bundles, also bundle diameters. The latter evaluation of diameters relies, however, on the validity of results from theoretical models. In fact, turning

$$\langle\nu(\epsilon)\rangle = \frac{\sum_{j=1}^{8}(I_j + 10^{-7} * \int_{a_{j+}}^{a_{j+1}-}[\nu_{\mathrm{RBM}} + C_2(N,d)]\,\rho(d)\exp[-(d-d_0)^2/2\sigma^2]\,\mathrm{d}d}{\sum_{j=1}^{8}(I_j + 10^{-7} * \int_{a_{j+}}^{a_{j+1}-}\rho(d)\exp[-(d-d_0)^2/2\sigma^2]\,\mathrm{d}d}, \tag{16}$$

the problem around, from known bundle diameters intertube interaction can be evaluated. The fine structure in the Raman response and in the optical response is due to a clustering of geometrically allowed diameters which again is a consequence of the nanoscopic sizes of the tubes.

For the work carried out at the Universität Wien the authors acknowledge the Austrian Fonds zur Förderung der Wissenschaflichen Forschung project 12924-TPH and the European network HPRN-CT-1999-00011 for financial support. T.P. acknowledges the ÖAW for an APART grant. For the work carried out at the Tokyo Metropolitan University support is acknowledged from the Japan Society for the Promotion of Science, Research for the Future Program and from a Grant-in-Aid for Scientific Research on the Priority Area "Fullerenes and Nanotubes" by the Ministry of Education, Science, and Culture of Japan.

## Appendix

The evaluation of the oscillation for very narrow diameter distributions can be performed from

*See equation (16) above*

with

$$I_j = \int_{a_{j-}}^{a_{j+}}[\nu_{\mathrm{RBM}} + C_2(N,d)]\,\rho(d)\exp\left[-(d-d_0)^2/2\sigma^2\right]\,\mathrm{d}d. \tag{17}$$

Note that the integration in equation (16) extends over the regions in between the van Hove singularities. The factor $10^{-7}$ is empirical. For lower values oscillations are not quenched for small values of $\sigma$ and for larger values the calculated diameters disagree with the experiment if $\sigma$ is specified in the experimental range.

## References

1. S. Iijima *et al.*, Nature **354**, 56 (1991).
2. A. Thess *et al.*, Science **273**, 483 (1996).
3. C. Journet *et al.*, Nature **388**, 756 (1997).
4. For a summary of the state of the art see the review articles: M.S. Dresselhaus *et al.*, *Science of Fullerenes and Carbon Nanotubes* (Academic Press, New York, 1996); R. Saito, G.Dresselhaus, M.S. Dresselhaus, Physical Properties of Carbon Nanotubes (Imperial College Press, London, 1998); M. Dresselhaus, P. Eklund, Adv. Phys. **49**, 705 (2000).
5. A. Rinzler *et al.*, Appl. Phys. A **67**, 29 (1998).
6. J.W.G. Wildöer *et al.*, Nature **381**, 59 (1998).
7. S. Rols *et al.*, Europ. Phys. J. B **10**, 263 (1999).
8. M. Milnera *et al.*, Phys. Rev. Lett. **84**, 1324 (2000).
9. M.A. Pimenta *et al.*, Phys. Rev. B **58**, R16016 (1998).
10. H. Kuzmany *et al.*, Europhys. Lett. **44**, 518 (1998).
11. O. Jost *et al.*, Appl. Phys. Lett. **75**, 2217 (1999).
12. H. Kataura *et al.*, Synth. Metals **103**, 2555 (1999).
13. H. Kataura *et al.*, Carbon **38**, 1691 (2000).
14. Z.K. Tang *et al.*, Appl. Phys. Lett. **73**, 2287 (1998).
15. C. Thomsen *et al.*, Phys. Rev. B **61**, 16179 (2000).
16. R. Saito *et al.*, Phys. Rev. B **61**, 2981 (2000).
17. M. Hulman *et al.*, Phys. Rev. **63**, 82406 (2001).
18. A.M. Rao *et al.*, Science **275**, 187 (1997).
19. D. Sanchez-Portal, Phys. Rev. B **59**, 12678 (1999).
20. J. Kürti *et al.*, Phys. Rev. B **58**, R8869 (1998).
21. U.D. Venkateswaran *et al.*, Phys. Rev. B **59**, 10928 (1999).
22. L. Henrard, Ph. Lambin, A. Rubio, *Proc. Int. Winterschool on Electronic Properties of Molecular Nanostructure*, Kirchberg 2000, p. 266, edited by H. Kuzmany *et al.*, AIP Conference Proceedings Vol. 544 (Melville, New York, 2000).
23. L. Henrard *et al.*, Phys. Rev. **60**, R8521 (1999).
24. R.M. Martin, L.M. Falicov, Topics Appl. Phys. **8**, 79 (1983).
25. H. Peterlik, P. Fratzl, K. Kromp, Carbon **32**, 820 (1994).
26. H. Peterlik, unpublished.
27. B.E. Warren, Phys. Rev. B **59**, 693 (1941).
28. R.E. Franklin, Acta Cryst. **4**, 253 (1951).
29. A. Guinier, G. Fournet, *Small-angle scattering of X-rays* (Chapman & Hall Ltd., 1955), pp. 5–30.
30. X. Blase *et al.*, Phys. Rev. Lett. **72**, 1878 (1994).
31. Ando *et al.*, J. Phys. Soc. Jpn **66**, 1066 (1998).
32. M. Ichida *et al.*, J. Phys. Soc. Jpn **68**, 3131 (1999).
33. V. Popov (2000), private communication.